

On the Stability of an Electrostatically-Actuated Functionally Graded Magneto-Electro-Elastic Micro-Beams Under Magneto-Electric Conditions

A. Amiri^{*}, G. Rezazadeh, R. Shabani, A. Khanchehgardan

Mechanical Engineering Department, Urmia University, Urmia, Iran

Received 15 July 2016; accepted 20 September 2016

ABSTRACT

In this paper, the stability of a functionally graded magneto-electro-elastic (FG-MEE) micro-beam under actuation of electrostatic pressure is studied. For this purpose Euler-Bernoulli beam theory and constitutive relations for magneto-electro-elastic (MEE) materials have been used. We have supposed that material properties vary exponentially along the thickness direction of the micro-beam. Governing motion equations of the micro-beam are derived by using of Hamilton's principle. Maxwell's equation and magneto-electric boundary conditions are used in order to determine and formulate magnetic and electric potentials distribution along the thickness direction of the micro-beam. By using of magneto-electric potential distribution, effective axial forces induced by external magneto-electric potential are formulated and then the governing motion equation of the micro-beam under electrostatic actuation is obtained. A Galerkin-based step by step linearization method (SSLM) has been used for static analysis. For dynamic analysis, the Galerkin reduced order model has been used. Static pull-in instability for 5 types of MEE micro-beam with different gradient indexes has been investigated. Furthermore, the effects of external magneto-electric potential on the static and dynamic stability of the micro-beam are discussed in detail.

© 2016 IAU, Arak Branch. All rights reserved.

Keywords : Functionally graded; MEE; MEMS; Maxwell's Equation; Pull-in instability.

1 INTRODUCTION

SMART structures constructed from smart materials, have absorbed much attentions of researchers and scientists in recent years. Smart or intelligent materials such as piezoelectric, piezomagnetic, magnetostrictive and so others, are finding numerous applications in broad- range of technological fields such as nano-scale technology, sensors, actuators and many others. These materials have a unique ability of self-sensing and adaptive capabilities [1- 5]. There is a coupling effect and interactions between different fields in these materials that allow them to convert energy from one type to the other [6,7]. One of the most important smart materials is MEE materials. MEE composite materials are made of piezo-electric and piezo-magnetic phases, which allow them to exhibit three-phase coupling effect between magnetic, electric and mechanical fields, in the other words they have novel property of converting energy from one form to the other among magnetic, electric and mechanical energies [8-12]. Because of these magneto-electricity properties of these new smart composite materials (MEE) which cannot

^{*}Corresponding author. Tel.: +98 9148406141.
E-mail address: amiri.ahd@gmail.com (A. Amiri).

be found in the single-phase piezo-electric and piezo-magnetic materials, they have attracted more attentions [13-15]. An example of such a composite is piezoelectric Barium Titanate (BaTiO_3) embedded in a matrix of magnetostrictive Cobalt Iron Oxide (CoFeO_4).

During the last several years, the magneto-electro-mechanical coupling problems which are associated with the reputed MEE materials have been developed by many researchers and authors. These composite materials have concomitantly piezoelectric, piezo-magnetic and magneto-electric effects [16-19]. Li [16] investigated buckling analysis of MEE plate resting on Pasternak foundation. They have used mindlin theory, Maxwell's equation and variational principle for modeling the problem. In numerical results, they have investigated the effects of magneto-electric potential, Pasternak shear coefficients and Winkler spring on the buckling load. Ke and Wang [10] investigated the free vibration of MEE nano-beams based on the nonlocal theory and Timoshenko beam theory. In their study, the MEE nano-beam is under the external magneto-electric potential and constant temperature change. They have used the differential quadrature (DQ) method in order to investigate the natural frequencies and mode shapes. Furthermore, they have studied the effects of nonlocal parameter, temperature change and magneto-electric potential on the size-dependent vibration characteristics of MEE nano-beams. Xue et al [8] investigated the large deflection of a rectangular MEE thin plate. In their investigation, the nonlinear partial differential equation has been derived using Von Karman plate theory of large deflection. They have used Bubnov-Galerkin method for transforming the governing nonlinear equation to third-order nonlinear algebraic equation for the maximum deflection. In addition, the coupling factor has been introduced in order to determine the coupling effect on deflections. Milazzo [20] derived a model for the large deflection analysis of MEE laminated plates. They have employed first order shear deformation theory and Von Karman stress function approach and investigated the influence of large deflection on the plate response.

On the other hands, functionally graded materials (FGM) have been rapidly growing during recent years. Some studies have been performed by researchers on the mechanical behavior of FG-MEE structures. Huang et al [13] presented an analytical solution for FG-MEE plane beams. They have assumed that the properties of the MEE material vary arbitrarily along the thickness direction and obtained the analytical solutions for beams under tension and pure bending, for cantilever beams subjected to shear force applied at the free end, and for cantilever beams subjected to uniform load. Xue and Pan [21] studied the wave propagation in FG-MEE long and circular rod made of piezoelectric BaTiO_3 and piezomagnetic CoFe_2O_4 . They have assumed that the material properties vary exponentially along the rod direction and derived one-dimensional wave-motion equation for the problem. In numerical results, they have studied the effect of the gradient factor and material coupling on the wave features. In addition they have calculated the effective Young's modulus and effective Poisson's ratio in the BaTiO_3 - CoFe_2O_4 composite rod.

Micro-cantilevers and clamped-clamped micro-beams are used extensively in micro-electro-mechanical systems (MEMS). There are various actuation methods in such systems, but electrostatic actuation is the most popular actuation mechanism used in micro/nano electromechanical systems (NEMS/MEMS), and this is due to its many intrinsic advantages. These systems contain two electrodes, which one of them is fixed and the other one is movable. When the applied voltage exceeds a critical value, the movable micro-beam becomes unstable and is pulled into the fixed electrode. Pull-in phenomenon is very important in designing such systems [22-27]. This phenomenon has been investigated by many researchers in recent years for micro structures made of different materials. In nano-scale structures, intermolecular forces such as Casimir force and Van der Waals force can play a crucial role in the deflection and pull-in performance. These forces depend on the gap between beam and substrate. When the gap between beam and substrate is large enough (larger than 20 nm, and below 1000 nm), the intermolecular force is simplified as the Casimir force. Casimir force is not affected by material properties. Van der Waals force is important when the gap between the electrodes is less than 20 nm [28-31].

In this paper, due to importance of smart materials in mechanical systems, the stability behavior of electrostatically-actuated FG-MEE micro-beam is studied. In fact the novelty of this paper is employing of the FG-MEE materials in MEMS structures. Due to adaptive and controllable properties of MEE materials, we can control the pull-in instability in the system. For numerical analysis, an Euler-Bernoulli clamped-clamped FG-MEE micro-beam is considered. Constitutive relations for MEE materials, Maxwell's equation and Hamilton's principle have been used in order to model the problem. In numerical results, we have investigated the static and dynamic mechanical behavior of the system. Furthermore, the effects of magneto-electric external potential on the pull-in phenomenon are discussed. Present paper and its results may be useful for development of smart MEMS structures which have attracted more attentions of researchers in recent years.

2 MODEL DESCRIPTIONS

2.1 Euler-Bernoulli beam theory

According to the coordinate system (x, z) , shown in Fig.1, the displacement components in the Euler-Bernoulli beam can be represented as following:

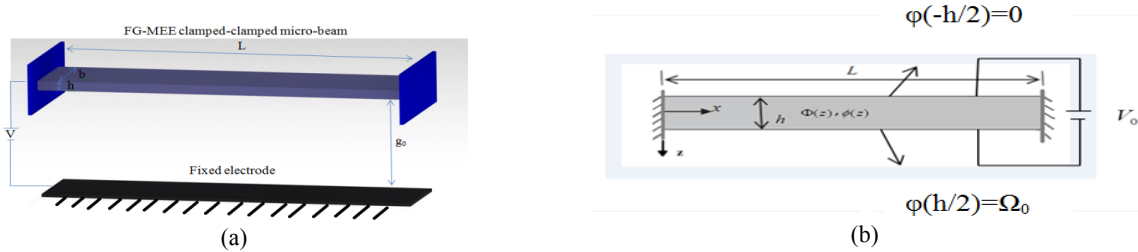


Fig.1

Schematic view of an electro-statically actuated FG-MEE micro-beam; (a) Clamped-Clamped FG-MEE micro-beam ;(b) Side view of the micro-beam under external magneto- electric potential.

$$u(x, z, t) = -z \frac{\partial w}{\partial x}, v(x, z, t) = 0, w(x, z, t) = w(x, t) \quad (1)$$

where u , v and w , are respectively, the x - , y - , and z - components of displacement vector. So the strains associated with the above displacement field of the micro-beam can be expressed in the following form:

$$\varepsilon_{xx} = -z \frac{\partial^2 w}{\partial x^2}, \varepsilon_{yy} = \varepsilon_{zz} = \gamma_{xz} = \gamma_{xy} = \gamma_{yz} = 0 \quad (2)$$

In which ε and γ are the normal and shear strains, respectively.

2.2 Mathematical modeling

For a beam made from transversely isotropic FG-MEE material, we suppose that the material properties vary exponentially along the thickness direction as [21]:

$$c_{ij} = c_{ij}^0 e^{\alpha z}, e_{ij} = e_{ij}^0 e^{\alpha z}, h_{ij} = h_{ij}^0 e^{\alpha z}, f_{ij} = f_{ij}^0 e^{\alpha z}, g_{ij} = g_{ij}^0 e^{\alpha z}, \mu_{ij} = \mu_{ij}^0 e^{\alpha z}, \rho_{ij} = \rho^0 e^{\alpha z} \quad (3)$$

where the constant factor of the material property is denoted by superscript 0; c_{ij} , e_{ij} , h_{ij} , f_{ij} , g_{ij} , μ_{ij} and ρ denote elastic, piezoelectric, dielectric, piezomagnetic, magneto-electric and magnetic permeability constants and the density of the material, respectively; α is the gradient index of the material.

The constitutive relations for a Homogeneous MEE solid can be written as [10]:

$$\sigma_{ij} = c_{ijkl} \varepsilon_{kl} - e_{mij} E_m - f_{nij} H_n, \quad (4)$$

$$D_i = e_{ikl} \varepsilon_{kl} + h_{im} E_m + g_{in} H_n, \quad (5)$$

$$B_i = f_{ikl} \varepsilon_{kl} + g_{im} E_m + \mu_{in} H_n. \quad (6)$$

where σ_{ij} is the stress component; D_i and B_i are the electric displacement and magnetic induction, respectively; E_i and H_i are the electric and magnetic field intensities, respectively.

Based on the Maxwell's equation, the electric and magnetic intensities can be expressed as gradients of the scalar electric and magnetic potentials Φ and φ , respectively as following:

$$E_z = -\frac{\partial\phi}{\partial z}; E_x = -\frac{\partial\phi}{\partial x} \tag{7}$$

$$H_z = -\frac{\partial\varphi}{\partial z}; H_x = -\frac{\partial\varphi}{\partial x} \tag{8}$$

Considering Eqs. (4), (5) and (6), the constitutive relations for MEE beam can be written as:

$$\sigma_{xx} = c_{11}\varepsilon_{xx} - e_{31}E_z - f_{31}H_z, \tag{9}$$

$$D_z = e_{31}\varepsilon_{xx} + h_{33}E_z + g_{33}H_z, \tag{10}$$

$$B_z = f_{31}\varepsilon_{xx} + g_{33}E_z + \mu_{33}H_z, \tag{11}$$

$$D_x = h_{11}E_x + g_{11}H_x, \tag{12}$$

$$B_x = g_{11}E_x + \mu_{11}H_x. \tag{13}$$

The in-plane magnetic and electric fields can be neglected for a thin beam, in the other words $E_x = H_x = 0$. According to this assumption, we can write the strain energy of the beam as following:

$$U_e = \frac{1}{2} \int_0^l \int_{-h/2}^{h/2} (\sigma_{xx}\varepsilon_{xx} - D_z E_z - B_z H_z) dz dx \tag{14}$$

Considering relations (2), (7) and (8), Eq. (14), can be rewritten as following:

$$U_e = -\frac{1}{2} \int_0^l (M_{xx} \frac{\partial^2 w}{\partial x^2}) dx + \frac{1}{2} \int_0^l \int_{-h/2}^{h/2} (D_z \frac{\partial\phi}{\partial z} + B_z \frac{\partial\varphi}{\partial z}) dz dx \tag{15}$$

where M_{xx} is the bending moment which can be calculated from Eq. (16).

$$M_{xx} = \int_{-h/2}^{h/2} \sigma_{xx} z dz \tag{16}$$

Neglecting the micro-rotations, the kinetic energy U_T can be expressed as [32]:

$$U_T = \frac{1}{2} \int_0^l (\overline{\rho h}) (\frac{\partial w}{\partial t})^2 dx \tag{17}$$

where:

$$\overline{\rho h} = \int_{-h/2}^{h/2} \rho^0 e^{\alpha z} dz = \frac{2\rho^0}{\alpha} \text{Sinh}(\frac{\alpha h}{2}) \tag{18}$$

The work done by the external electric and magnetic potentials can be calculated from Eq. (19) [10].

$$U_F = \frac{1}{2} \int_0^l (N_e + N_m) (\frac{\partial w}{\partial x})^2 dx \tag{19}$$

where N_m and N_e are the normal axial force generated by the external magnetic and electric potentials respectively. The variation of work done by the electrostatic force can be denoted as:

$$\delta W_q = \int_0^l (\bar{q}_{elect} \delta w) dx \quad (20)$$

where \bar{q}_{elect} is the electrostatic force between micro-beam and substrate, which can be expressed as [33]:

$$\bar{q}_{elect} = \frac{\epsilon_0 V^2}{2(g_0 - w)^2} \quad (21)$$

where $\epsilon_0 = 8.854 \times 10^{-12} \text{ C}^2 \text{ N}^{-1} \text{ m}^{-2}$ is the permittivity of vacuum within the gap, V is the electric potential difference between the beam and the substrate, g_0 is initial gap between beam and substrate.

Now the Hamilton's principle is considered:

$$\int_0^t (\delta U_T - \delta U_e + \delta W_q + \delta U_F) dt = 0 \quad (22)$$

By substituting Eqs. (15), (17), (19) and (20) into (22), integrating by parts and setting the coefficients of $\delta w, \delta \phi, \delta \varphi$ to zero, the governing equations of the beam are derived as following [10]:

$$-\left(\frac{\partial^2 M_{xx}}{\partial x^2}\right) + (N_m + N_e) \frac{\partial^2 w}{\partial x^2} + \rho h \frac{\partial^2 w}{\partial t^2} = \bar{q}_{elect} \quad (23)$$

$$\frac{\partial}{\partial z}(D_z) = 0 \quad (24)$$

$$\frac{\partial}{\partial z}(B_z) = 0 \quad (25)$$

Considering Eqs. (3), (7), (8), (10) and (11) and applying them to Eqs. (24) and (25), the following equations are obtained:

$$-e_{31}^0 \frac{\partial^2 w}{\partial x^2} - \alpha e_{31z}^0 \frac{\partial^2 w}{\partial x^2} - \alpha h_{33}^0 \frac{\partial \phi}{\partial z} - h_{33}^0 \frac{\partial^2 \phi}{\partial z^2} - \alpha g_{33}^0 \frac{\partial \varphi}{\partial z} - g_{33}^0 \frac{\partial^2 \varphi}{\partial z^2} = 0 \quad (26)$$

$$-f_{31}^0 \frac{\partial^2 w}{\partial x^2} - \alpha f_{31z}^0 \frac{\partial^2 w}{\partial x^2} - \alpha g_{33}^0 \frac{\partial \phi}{\partial z} - g_{33}^0 \frac{\partial^2 \phi}{\partial z^2} - \alpha \mu_{33}^0 \frac{\partial \varphi}{\partial z} - \mu_{33}^0 \frac{\partial^2 \varphi}{\partial z^2} = 0 \quad (27)$$

Eqs. (26) and (27) can be represented as following matrix form:

$$\begin{pmatrix} h_{33}^0 & g_{33}^0 \\ g_{33}^0 & \mu_{33}^0 \end{pmatrix} \begin{Bmatrix} \frac{\partial^2 \phi}{\partial z^2} + \alpha \frac{\partial \phi}{\partial z} \\ \frac{\partial^2 \varphi}{\partial z^2} + \alpha \frac{\partial \varphi}{\partial z} \end{Bmatrix} = \begin{Bmatrix} e_{31}^0 + \alpha z e_{31}^0 \\ f_{31}^0 + \alpha z f_{31}^0 \end{Bmatrix} \times \frac{-\partial^2 w}{\partial x^2} \quad (28)$$

Referring to the Cramer's rule for the matrix equations, we can obtain the following equations:

$$\frac{\partial^2 \phi}{\partial z^2} + \alpha \frac{\partial \phi}{\partial z} = \frac{\begin{vmatrix} e_{31}^0 + \alpha z e_{31}^0 & g_{33}^0 \\ f_{31}^0 + \alpha z f_{31}^0 & \mu_{33}^0 \end{vmatrix}}{\begin{vmatrix} h_{33}^0 & g_{33}^0 \\ g_{33}^0 & \mu_{33}^0 \end{vmatrix}} \cdot \frac{-\partial^2 w}{\partial x^2} \tag{29}$$

$$\frac{\partial^2 \varphi}{\partial z^2} + \alpha \frac{\partial \varphi}{\partial z} = \frac{\begin{vmatrix} h_{33}^0 e_{31}^0 + \alpha z e_{31}^0 \\ g_{33}^0 f_{31}^0 + \alpha z f_{31}^0 \end{vmatrix}}{\begin{vmatrix} h_{33}^0 & g_{33}^0 \\ g_{33}^0 & \mu_{33}^0 \end{vmatrix}} \cdot \frac{-\partial^2 w}{\partial x^2} \tag{30}$$

Eqs. (29) and (30) can be rewritten as the form as Eqs. (31) and (32), respectively.

$$\frac{\partial^2 \phi}{\partial z^2} + \alpha \frac{\partial \phi}{\partial z} = -M_1^0 (1 + \alpha z) \frac{\partial^2 w}{\partial x^2} \tag{31}$$

$$\frac{\partial^2 \varphi}{\partial z^2} + \alpha \frac{\partial \varphi}{\partial z} = -M_2^0 (1 + \alpha z) \frac{\partial^2 w}{\partial x^2} \tag{32}$$

where:

$$M_1^0 = \frac{e_{31}^0 \mu_{33}^0 - f_{31}^0 g_{33}^0}{h_{33}^0 \mu_{33}^0 - g_{33}^0{}^2}, M_2^0 = \frac{h_{33}^0 f_{31}^0 - e_{31}^0 g_{33}^0}{h_{33}^0 \mu_{33}^0 - g_{33}^0{}^2} \tag{33}$$

Considering boundary conditions of the external magneto-electric potential represented by Eq. (34), solving Eqs. (31) and (32) according to this assumption that gradient index α is positive ($\alpha > 0$), distribution of the electric and magnetic potentials along the thickness direction of the micro-beam can be obtained as following:

$$\phi(h/2) = V_0, \phi(h/2) = \Omega_0, \phi(-h/2) = \varphi(-h/2) = 0. \tag{34}$$

$$\phi = \frac{-M_1^0}{2} \frac{\partial^2 w}{\partial x^2} \left(z^2 - \left(\frac{h}{2}\right)^2 \right) - \frac{V_0}{2 \text{Sinh}(\alpha \frac{h}{2})} e^{-\alpha z} + \frac{V_0}{2 \text{Sinh}(\alpha \frac{h}{2})} e^{\alpha \frac{h}{2}} \tag{35}$$

$$\varphi = \frac{-M_2^0}{2} \frac{\partial^2 w}{\partial x^2} \left(z^2 - \left(\frac{h}{2}\right)^2 \right) - \frac{\Omega_0}{2 \text{Sinh}(\alpha \frac{h}{2})} e^{-\alpha z} + \frac{\Omega_0}{2 \text{Sinh}(\alpha \frac{h}{2})} e^{\alpha \frac{h}{2}} \tag{36}$$

Substituting Eqs. (2), (35), and (36) into Eq. (9), using Eq. (16), the following result is obtained:

$$M_{xx} = -(c_{11}^0 + e_{31}^0 M_1^0 + f_{31}^0 M_2^0) \frac{\partial^2 w}{\partial x^2} \int_{-h/2}^{h/2} z^2 e^{\alpha z} dz \tag{37}$$

Eq. (37) can be rewritten as the form of following equation:

$$M_{xx} = -(c_{11}^0 + e_{31}^0 M_1^0 + f_{31}^0 M_2^0) \frac{\partial^2 w}{\partial x^2} \left\{ \left(\frac{h^2}{2\alpha} + \frac{4}{\alpha^3} \right) \text{Sinh}(\alpha \frac{h}{2}) - \frac{2h}{\alpha^2} \text{Cosh}(\alpha \frac{h}{2}) \right\} \tag{38}$$

By attention to Eq. (9), generated axial forces caused by external electric and magnetic potentials can be calculated from:

$$N_e = \int_{-h/2}^{h/2} e_{31} E_z dz, N_m = \int_{-h/2}^{h/2} f_{31} H_z dz \quad (39)$$

According to Eqs. (35) and (36) and using Eqs. (7), (8), (39), the effective normal forces induced by the external electric and magnetic potentials are formulated as following:

$$N_e = -\frac{V_0 e_{31}^0 \alpha h}{2 \text{Sinh}(\alpha \frac{h}{2})}, N_m = -\frac{\Omega_0 f_{31}^0 \alpha h}{2 \text{Sinh}(\alpha \frac{h}{2})}. \quad (40)$$

Substituting Eq. (38) into Eq. (23), the governing motion equation of FG-MEE Euler-Bernoulli beam under electrostatic actuation is obtained as:

$$(c_{11}^0 + e_{31}^0 M_1^0 + f_{31}^0 M_2^0) \left\{ \left(\frac{h^2}{2\alpha} + \frac{4}{\alpha^3} \right) \text{Sinh}(\alpha \frac{h}{2}) - \frac{2h}{\alpha^2} \text{Cosh}(\alpha \frac{h}{2}) \right\} \frac{\partial^4 w}{\partial x^4} + (N_m + N_e) \frac{\partial^2 w}{\partial x^2} + \rho h \frac{\partial^2 w}{\partial t^2} = \frac{\varepsilon_0 V^2}{2(g_0 - w)^2} \quad (41)$$

Non-dimensional parameters represented in Eq. (42), are used in order to write Eq. (41) in non-dimensional form.

$$\hat{w} = \frac{w}{g_0}; \hat{x} = \frac{x}{L}; \hat{t} = \frac{t}{t^*}; t^* = \sqrt{\frac{\rho h L^4}{\tilde{c}_{11} \left\{ \left(\frac{h^2}{2\alpha} + \frac{4}{\alpha^3} \right) \text{Sinh}(\alpha \frac{h}{2}) - \frac{2h}{\alpha^2} \text{Cosh}(\alpha \frac{h}{2}) \right\}}} \quad (42)$$

$$\tilde{c}_{11} = c_{11}^0 + e_{31}^0 M_1^0 + f_{31}^0 M_2^0 \quad (43)$$

In which the variables with hat are the non-dimensional values of the related parameters and t^* is a characteristic time. So Eq. (41) can be changed as:

$$\frac{\partial^4 \hat{w}}{\partial \hat{x}^4} + \frac{\partial^2 \hat{w}}{\partial \hat{t}^2} + (\lambda_1 + \lambda_2) \frac{\partial^2 \hat{w}}{\partial \hat{x}^2} = \lambda_3 \frac{V^2}{(1 - \hat{w})^2} \quad (44)$$

where

$$\lambda_1 = N_m \frac{L^2}{\tilde{c}_{11} \left\{ \left(\frac{h^2}{2\alpha} + \frac{4}{\alpha^3} \right) \text{Sinh}(\alpha \frac{h}{2}) - \frac{2h}{\alpha^2} \text{Cosh}(\alpha \frac{h}{2}) \right\}}; \quad (45)$$

$$\lambda_2 = N_e \frac{L^2}{\tilde{c}_{11} \left\{ \left(\frac{h^2}{2\alpha} + \frac{4}{\alpha^3} \right) \text{Sinh}(\alpha \frac{h}{2}) - \frac{2h}{\alpha^2} \text{Cosh}(\alpha \frac{h}{2}) \right\}}; \quad (46)$$

$$\lambda_3 = \frac{\varepsilon_0 L^4}{2 \tilde{c}_{11} \left\{ \left(\frac{h^2}{2\alpha} + \frac{4}{\alpha^3} \right) \text{Sinh}(\alpha \frac{h}{2}) - \frac{2h}{\alpha^2} \text{Cosh}(\alpha \frac{h}{2}) \right\} g_0^3}. \quad (47)$$

The static equation can be written as following:

$$\frac{\partial^4 \hat{w}}{\partial \hat{x}^4} + (\lambda_1 + \lambda_2) \frac{\partial^2 \hat{w}}{\partial \hat{x}^2} = \lambda_3 \frac{V^2}{(1 - \hat{w})^2} \tag{48}$$

3 NUMERICAL APPROACH

3.1 Static analysis

For numerical analysis of the problem, SSLM is used to linearize Eq. (48). When this equation is linearized, it can be solved by using of the Galerkin-based weighted residual method. According to SSLM, the voltage applied between the micro-beam and substrate is increased from zero to the final value gradually. By assumption of superscript ‘i’ as the step counter, the deflection at (i + 1)th step can be obtained as:

$$V^{i+1} = V^i + \delta V, \hat{w}^{i+1} = \hat{w}^i + \psi \tag{49}$$

where ψ is the deflection growth.

According to Eq. (48), static deflection of the micro-beam at (i + 1)th step can be expressed as:

$$\frac{\partial^4 \hat{w}^{i+1}}{\partial \hat{x}^4} + (\lambda_1 + \lambda_2) \frac{\partial^2 \hat{w}^{i+1}}{\partial \hat{x}^2} = \lambda_3 \left(\frac{V^{i+1}}{1 - \hat{w}^{i+1}} \right)^2 \tag{50}$$

Substituting Eq. (49) into Eq. (50), using Taylor’s expansion and keeping first two terms of expansion in each step, following result can be obtained:

$$\frac{\partial^4 \psi}{\partial \hat{x}^4} + (\lambda_1 + \lambda_2) \frac{\partial^2 \psi}{\partial \hat{x}^2} - 2\lambda_3 \frac{(V^i)^2}{(1 - \hat{w}^i)^3} \psi - 2\lambda_3 \frac{V^i}{(1 - \hat{w}^i)^2} \delta V - 4\lambda_3 \frac{V^i}{(1 - \hat{w}^i)^3} \psi \delta V = 0 \tag{51}$$

In order to solve Eq. (51), ψ is expressed as following:

$$\psi(\hat{x}) = \psi_N(\hat{x}) = \sum_{j=1}^N a_j \beta_j(\hat{x}) \tag{52}$$

$\beta_j(\hat{x})$ is the suitable j^{th} shape function satisfying all of boundary conditions of the micro-beam, which can be defined as [33]:

$$\beta_j(\hat{x}) = (\cos(\Lambda_j \hat{x}) - \cosh(\Lambda_j \hat{x})) - P_j (\sin(\Lambda_j \hat{x}) - \sinh(\Lambda_j \hat{x})), \tag{53}$$

where:

$$P_j = \frac{(\cos(\Lambda_j) - \cosh(\Lambda_j))}{(\sin(\Lambda_j) - \sinh(\Lambda_j))}; \Lambda_j = 4.73, 7.85, 10.99, 14.137 \tag{54}$$

Applying Eq. (52) into Eq. (51), multiplying the result by $\beta_i(\hat{x})$ as a weight function in the Galerkin method and calculating the integrated from $\hat{x} = 0$ to 1, a set of equations is obtained. By solving these equations, static deflection of the micro-beam and consequently static pull-in voltage can be determined. Numerical results for this analysis have been presented in next section.

3.2 Dynamic analysis

In order to investigate the dynamic instability behavior of the micro-beam, dynamic deflection can be expressed as:

$$\hat{w}(\hat{x}, t) \cong \sum_{j=1}^N q_j(\hat{t}) \beta_j(\hat{x}) \quad (55)$$

where $q_j(\hat{t})$ is the time dependent generalized coordinate.

Substituting Eq. (55) into Eq. (44), multiplying the result by $\beta_i(\hat{x})$ and integrating from $\hat{x} = 0$ to 1, following result can be obtained:

$$\sum_{j=1}^N M_{ij} \ddot{q}_j(\hat{t}) + \sum_{j=1}^N (K_{ij}^a + K_{ij}^b) q_j(\hat{t}) = F_i \quad (56)$$

$M_{ij}, K_{ij}^a, K_{ij}^b$ and F_i are given as:

$$M_{ij} = \int_0^1 \beta_i \beta_j d\hat{x}; K_{ij}^a = \int_0^1 \beta_i \beta_j^{(IV)} d\hat{x}; K_{ij}^b = \int_0^1 (\lambda_1 + \lambda_2) \beta_i \beta_j^{(2)} d\hat{x}; F_i = \int_0^1 \frac{\lambda_3 V^2}{(1 - \hat{w}(\hat{x}, \hat{t}))^2} \beta_i d\hat{x} \quad (57)$$

It is worth pointing out that Eq. (56) can be solved by one of the numerical integration methods such as Runge-Kutta method.

In order to demonstrate the accuracy of the proposed method and verify it, the pull-in voltages of a silicon-made fixed-fixed micro-beam are compared with the results reported in Ref. [34]. The geometrical properties of the considered micro-beam are listed in Table 1. The calculated results are presented in Table 2. As it is seen, the results of SSLM agree well with the results in Ref. [34].

Table 1
Geometrical properties of FG-MEE micro-beam.

Symbol	Parameters	Values
L	Length	250 (μm)
h	Thickness	3 (μm)
b	Width	50 (μm)
g_0	Initial gap	1 (μm)

Table 2
The obtained pull-in voltages for different step size for the applied voltage.

Step size of the applied voltage (dV)	Obtained pull-in voltage in this paper	Pull-in voltage in reference [34]
1	40	39.5
0.1	39.5	39.5
0.05	39.4	39.5
0.01	39.33	39.5
0.005	39.32	39.5

4 NUMERICAL RESULTS AND DISCUSSION

4.1 Model properties

Numerical results of the problem are presented in this section. For this purpose, a clamped-clamped FG-MEE micro-beam made of two-phase $BaTiO_3$ - $CoFe_2O_4$ composite with different volume fractions (V.F.) of $BaTiO_3$ is considered. For different volume fractions of $BaTiO_3$ in the composite, there are distinct effective properties for the MEE material which are listed in Table 3. [21]

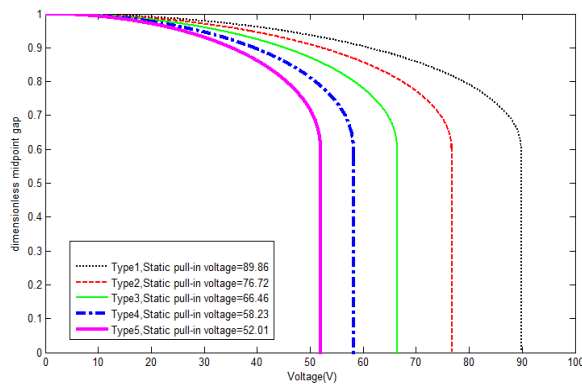
Table 3Properties of $BaTiO_3$ - $CoFe_2O_4$ composite material.

Type	1	2	3	4	5
V.F.	0%	25%	50%	75%	100%
C_{11}^0	286	245	213	187	166
C_{12}^0	173	139	113	93	77
C_{13}^0	170	138	113	93.8	78
C_{33}^0	269.5	235	207	183	162
C_{44}^0	45.3	47.6	49.9	52.1	43
e_{31}^0	0	-1.53	-2.71	-3.64	-4.4
e_{33}^0	0	4.28	8.86	13.66	18.6
e_{15}^0	0	0.05	0.15	0.46	11.6
h_{11}^0	0.08	0.13	0.24	0.53	11.2
h_{33}^0	0.093	3.24	6.37	9.49	12.6
μ_{11}^0	5.9	3.57	2.01	0.89	0.05
μ_{33}^0	1.57	1.21	0.839	0.47	0.1
f_{31}^0	580	378	222	100	0
f_{33}^0	700	476	292	136	0
g_{11}^0	0	-3.09	-5.23	-6.72	0
g_{33}^0	0	2334.15	2750	1847.49	0
ρ^0	5300	5430	5550	5660	5800

Unit: elastic constants, c_{ij} , in 10^9 N/m², piezoelectric constants, e_{ij} , in C/m², piezomagnetic constants, f_{ij} , in N/Am², dielectric constants, h_{ij} , in 10^{-9} C²/Nm², magnetic constants, μ_{ij} , in 10^{-6} Ns²/c², magneto-electric coefficients, g_{ij} , in 10^{-12} Ns/Vc and density, ρ , in Kg/m³.

4.2 Static pull-in analysis of the micro-beam, with no external electric/ magnetic potential ($\Omega_0 = V_0 = 0$) for various gradient index α in (μm^{-1})

The dimensionless midpoint deflections versus applied voltage, for the five types of FG-MEE clamped-clamped micro-beams and different gradient indexes are presented in Figs. (2), (3) and (4). As it is indicated in these figures, when electrostatic force caused by the applied voltage between two electrodes exceeds a critical value, the system will be unstable. Static instability which is known as pull-in phenomenon is shown in these figures in which at a particular voltage value, the movable micro-beam is suddenly pulled into the fixed electrode. Static pull-in voltages of the mentioned micro-beams are calculated and presented in these figures. Fig. 5 shows the variation of the static pull-in voltage versus volume fraction of $BaTiO_3$ in the MEE material. As expected, while the volume fraction of $BaTiO_3$ in the material increases, the pull-in voltage of the micro-beam decreases. This is due to the fact that, by enhancing the volume fraction of $BaTiO_3$, the effective Young's modulus of the micro-beam is decreased. By decreasing the effective Young's modulus, bending stiffness of the micro-beam is decreased and therefore micro-beam deflection versus voltage is increased and so the pull-in voltage decreases. The other result which can be obtained from this figure is that by increasing the gradient index of the FG-MEE material, the static pull-in voltage of the micro-beams increases drastically.

**Fig.2**

The non-dimensional midpoint deflection versus applied voltage (v) for gradient index $\alpha=1$.

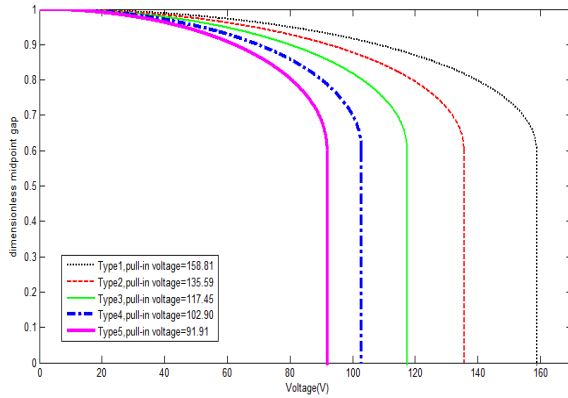


Fig.3
The non-dimensional midpoint deflection versus applied voltage (v) for gradient index $\alpha=2$.

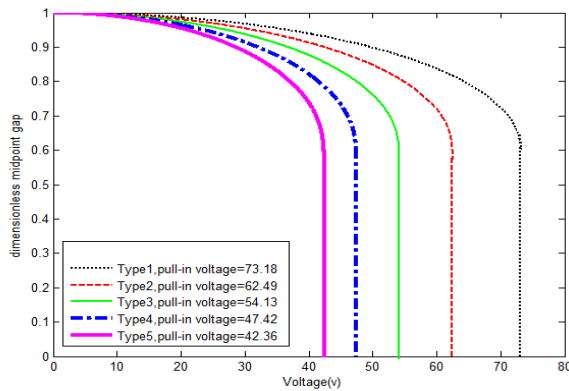


Fig.4
The non-dimensional midpoint deflection versus applied voltage (v) for gradient index 0.5.

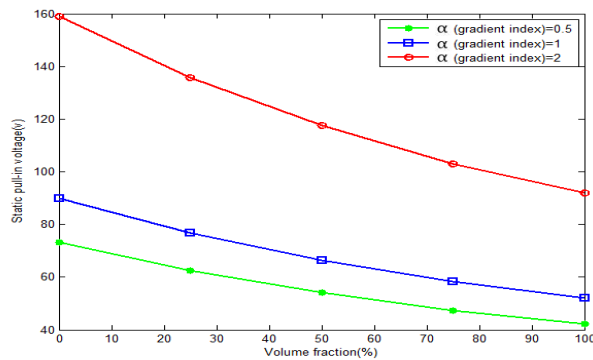


Fig.5
Static pull-in voltages versus volume fraction of $BaTiO_3$ in FG-MEE micro-beam for different gradient indexes.

4.3 Effects of the external magnetic potential Ω_0 and external electric potential V_0 on the pull-in instability of FG-MEE micro-beam

The non-dimensional midpoint deflection versus applied voltage (v) for FG-MEE micro-beams with gradient index of 1 ($\alpha = 1$) and 50% $BaTiO_3$ is presented in Fig.6. This figure shows the static pull-in instability for different values of external magnetic potential (Ω_0), and $V_0 = 0$. As it is shown, for a constant electrostatic voltage by increasing the external magnetic potential, the micro-beam deflection decreases and this is due to increasing the stiffness of the micro-beam. It can be obtained from this figure that by increasing the external magnetic potential Ω_0 , the pull-in voltage increases. Fig. 7 shows the static pull-in voltages for different values of external electric potential V_0 , and $\Omega_0 = 0$, for FG-MEE micro-beams with gradient index of 1 ($\alpha = 1$) and 50% $BaTiO_3$. This figure shows that, for a constant electrostatic voltage, when the applied external electric potential V_0 increases, the deflection of the micro-beam is increased. This is because of reducing the stiffness of the micro-beam which leads to

pull-in instability. This sensitivity of FG-MEE materials to the applied magneto-electric potential is due to the fact that the axial forces are generated in the micro-beams by the applied external magnetic and electric potentials. In the other words, by applying the external magneto-electric potential the stiffness of the micro-beams is changed. This property of FG-MEE smart materials can be useful for controlling the pull-in instability in the smart MEMS structures.

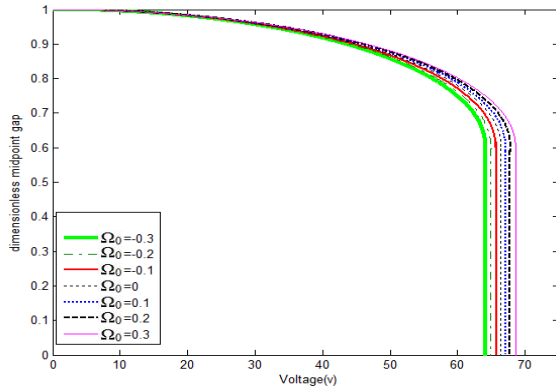


Fig.6 The non-dimensional midpoint deflection versus applied voltage (v) for gradient index 1, and various magnetic potential (Ω_0), $V_0 = 0$.

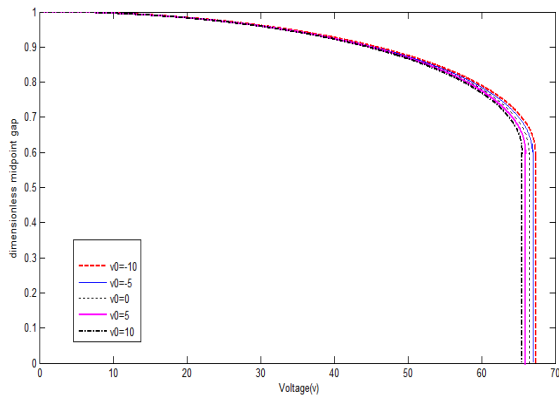


Fig.7 The non-dimensional midpoint deflection versus applied voltage (v) for gradient index 1, and various electric potential (V_0), $\Omega_0 = 0$.

Fig. 8 shows the effect of the external magnetic potential Ω_0 , on the pull-in voltage of FG-MEE micro-beam with gradient index of 1 ($\alpha = 1$) and $V_0 = 0$. This figure shows that, the pull-in voltage of FG-MEE micro-beam increases with the increase/decrease of the positive/negative external magnetic potential Ω_0 . This is due to the fact that the axial tensile and compressive forces are generated in micro-beam by the applied positive and negative magnetic potentials, respectively, in the other words by increasing/decreasing the applied positive/negative magnetic potential Ω_0 , the stiffness of micro-beam increases, so the pull-in voltage of FG-MEE micro-beam increases. One can understand from this figure that the effect of the external magnetic potential on the pull-in voltage decreases by increasing the volume fraction of piezoelectric phase in the FG-MEE material and this is due to the fact that piezomagnetic constant (f_{31}) is decreased in the material when the volume fraction changes from 0% to 100%.

Fig. 9 represents the effect of the external electric potential V_0 on the pull-in voltage of FG-MEE micro-beam with gradient index of 0.5 ($\alpha = 0.5$) and $\Omega_0 = 0$. Opposite of the effect of external magnetic potential, the pull-in voltage of FG-MEE micro-beam decreases with the increase/decrease of the positive/negative external electric potential V_0 because of generating the axial compressive and tensile forces, respectively. This figure shows that the effect of external electric potential on the pull-in voltage is increased when the volume fraction of $BaTiO_3$ in the FG-MEE material increases and this is due to increasing piezoelectric constant (e_{31}).

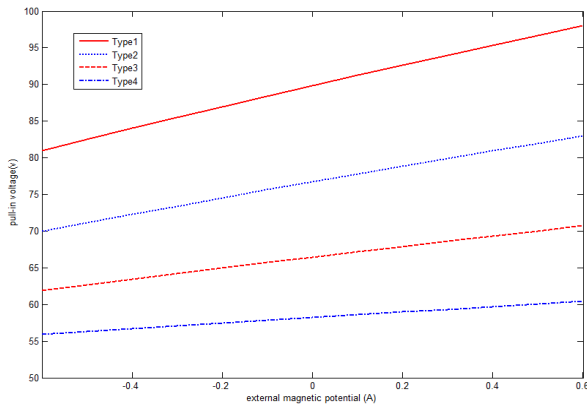


Fig.8
The effect of the external magnetic potential Ω_0 on the static pull-in voltage of FG-MEE micro-beam with $\alpha = 1$, $V_0 = 0$.

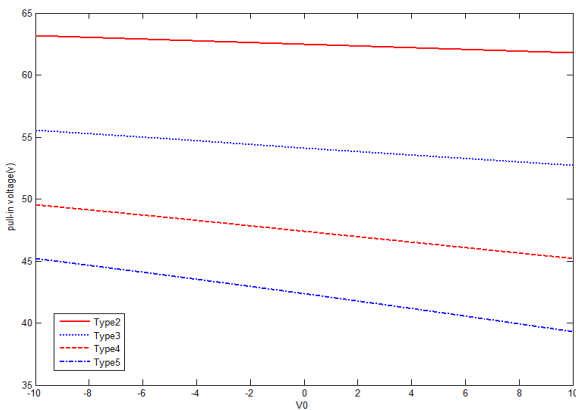


Fig.9
The effect of the external electric potential V_0 on the static pull-in voltage of FG-MEE micro-beam with $\alpha = 0.5$, $\Omega_0 = 0$.

The effect of applied external magnetic and electric potentials on the static pull-in voltages of the FG-MEE micro-beams with 50% volume fraction of $BaTiO_3$ for different values of gradient index is illustrated in Figs. (10) and (11), respectively. What is interesting in these figures is that, when the gradient index of the FG-MEE material increases, the effect of V_0 and Ω_0 on the pull-in instability of the micro-beam decreases. This is due to the fact that, for a constant magneto-electric potential, by increasing the gradient index α , the generated axial forces will be reduced (See Eq. (40)).

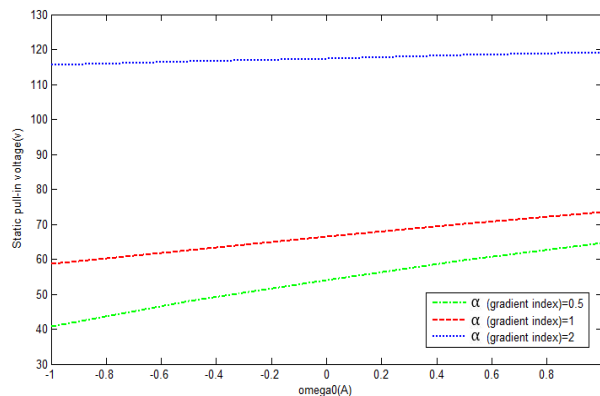


Fig.10
The effect of Ω_0 on the pull-in voltage of third type of FG-MEE micro-beam with $V_0 = 0$, for different values of α .

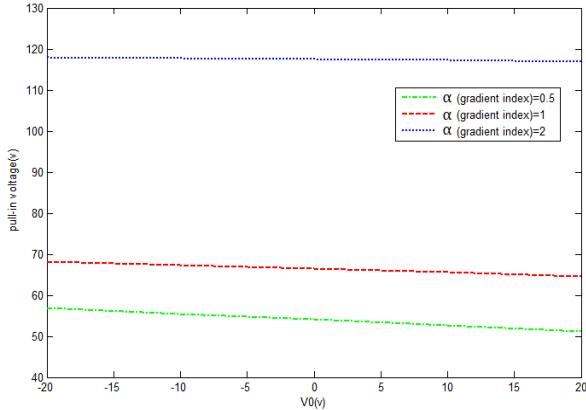


Fig.11
The effect of V_0 on the pull-in voltage of third type of FG-MEE micro-beam with $\Omega_0 = 0$, for different values of α .

Dynamic instability behavior of 4th type of FG-MEE micro-beam with gradient index of 0.5, subjected to constant step DC voltage (40v), for various external electric voltages V_0 is illustrated in Figs. (12), (13). As is evident, the response of the micro-beam to small positive V_0 is periodic. When V_0 increases, period of the vibrations increases and symmetry breaking in phase portrait happens, because of declining of the equivalent stiffness of micro-beam. In other words, when the positive V_0 is big enough, the system will be unstable.

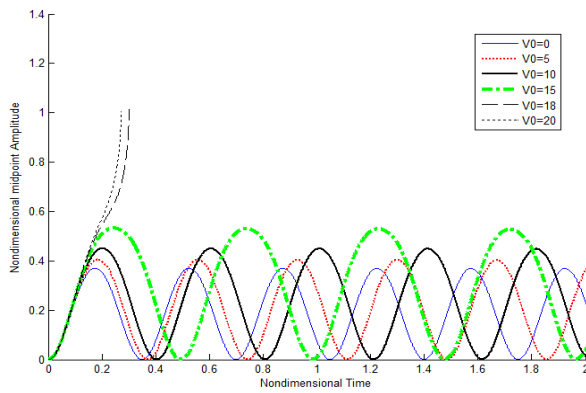


Fig.12
Time history of the 4th type of FG-MEE micro-beam for different values of V_0 with constant electrostatic voltage $V = 40v, \alpha = 0.5, \Omega_0 = 0$.

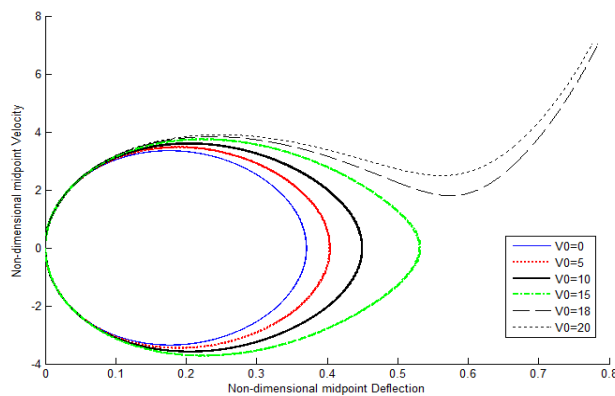


Fig.13
Phase portrait of the 4th type of FG-MEE micro-beam for different values of V_0 with constant electrostatic voltage $V = 40v, \Omega_0 = 0, \alpha = 0.5$.

Figs. (14) and (15) show the dynamic instability of the FG-MEE micro-beam with 75% volume fraction of $BaTiO_3$ and gradient index of 0.5, for different values of negative magnetic potential. As it can be obtained from these figures, by increasing of negative Ω_0 , dynamic instability occurs in the system, and this is due to this fact that by increasing negative Ω_0 , stiffness of the micro-beam decreases suddenly.

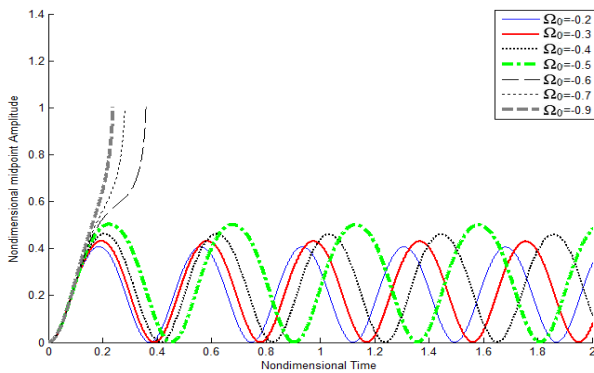


Fig.14
Time history of the 4th type of FG-MEE micro-beam for different values of Ω_0 with constant electrostatic voltage $V = 40\text{v}$, $\alpha = 0.5$, $V_0 = 0$.

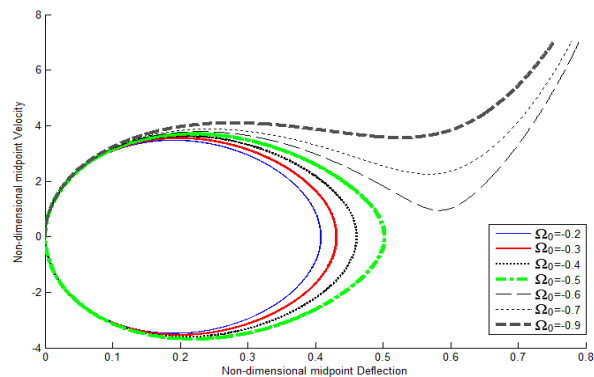


Fig.15
Phase portrait of the 4th type of FG-MEE micro-beam for different values of Ω_0 with constant electrostatic voltage $V = 40\text{v}$, $V_0 = 0$, $\alpha = 0.5$.

5 CONCLUSIONS

In the present work, the stability of electro-statically actuated FG-MEE micro-beams was studied. It was supposed that the properties of the FG-MEE material vary exponentially along the thickness direction of the micro-beam. Using Hamilton's principle, governing equations of the problem were derived. Maxwell's equation and magneto-electric boundary conditions was used in order to formulate the magnetic and electric potentials distribution along the thickness direction of the micro-beam. For static and dynamic analysis, the Galerkin-based step by step linearization method and Galerkin reduced order model was employed, respectively. From numerical results, following conclusions can be drawn: By increase of the volume fraction of piezoelectric phase in the FG-MEE material, the pull-in voltage is decreased. By increase of the gradient index, the pull-in voltage is increased. The pull-in voltage of the micro-beam decreases with the increase of the external electric potential (V_0), whereas the external magnetic potential (Ω_0) has the opposite effect, in the other words by increasing the external magnetic potential, the value of pull-in voltage of the micro-beam is increased. The effects of magnetic/electric potential on the pull-in instability of the FG-MEE micro-beams decrease/increase with the increase of the volume fraction of $BaTiO_3$ in the MEE material. By increase of the gradient index, the effect of magnetic and electric potentials on the pull-in instability decreases. It is worth to point out that the effects of electric and magnetic potentials on the dynamic instability of the micro-beams under constant electrostatic step DC voltage was investigated in detail by plotting time histories and phase portraits. This work and the obtained results could be used in the design and development of smart MEMS structures constructed from FG-MEE composite materials.

REFERENCES

- [1] Davi G., Milazzo A., 2011, A regular variational boundary model for free vibrations of magneto-electro-elastic structures, *Engineering Analysis with Boundary Elements* **35**: 303-312.

- [2] Fakhzan M.N., Muthalif Asan G.A., 2013, Harvesting vibration energy using piezoelectric material: Modeling, simulation and experimental verifications, *Mechatronics* **23**: 61-66.
- [3] Amiri A., Fakhari S.M., Pournaki I.J., Rezazadeh G., Shabani R., 2015, Vibration analysis of circular magneto-electro-elastic Nano-plates based on Eringen's nonlocal theory, *International Journal of Engineering, Transactions C: Aspects* **28**(12): 1808-1817.
- [4] Liu C., Ke L.L., Wang Y.S., Yang J., Kitipornchai S., 2013, Thermo-electro-mechanical vibration of piezoelectric nanoplates based on the nonlocal theory, *Composite Structures* **106**: 167-174.
- [5] Daga A., Ganesan N., Shankar K., 2009, Behavior of magneto-electro-elastic sensors under transient mechanical loading, *Sensors and Actuators A: Physical* **150**: 46-55.
- [6] Li Y.S., Cai Z.Y., Shi S.Y., 2014, Buckling and free vibration of magneto-electro-elastic nanoplate based on nonlocal theory, *Composite Structures* **111**: 522-529.
- [7] Linnemann K., Klinkel S., Wagner W., 2009, A constitutive model for magnetostrictive and piezoelectric materials, *International Journal of Solids and Structures* **46**: 1149-1166.
- [8] Xue C.X., Pan E., Zhang S.Y., 2011, Large deflection of a rectangular magneto-electro-elastic thin plate, *Mechanics Research Communications* **38**: 518-523.
- [9] Pan E., Heyliger P.R., 2003, Exact solutions for magneto-electro-elastic laminates in cylindrical bending, *International Journal of Solids and Structures* **40**: 6859-6876.
- [10] Ke L.L., Wang Y.S., 2014, Free vibration of size-dependent magneto-electro-elastic nanobeams based on the nonlocal theory, *Physica E* **63**: 52-61.
- [11] Amiri A., Pournaki I.J., Jafarzadeh E., Shabani R., Rezazadeh G., 2016, Vibration and instability of fluid-conveyed smart micro-tubes based on magneto-electro-elasticity beam model, *Microfluidics and Nanofluidics* **20**(2): 1-10.
- [12] Liu M.F., 2011, An exact deformation analysis for the magneto-electro-elastic fiber-reinforced thin plate, *Applied Mathematical Modelling* **35**: 2443-2461.
- [13] Huang D.J., Ding H.J., Chen W.Q., 2007, Analytical solution for functionally graded magneto-electro-elastic plane beams, *International Journal of Engineering Science* **45**: 467-485.
- [14] Chang T.P., 2013, On the natural frequency of transversely isotropic magneto-electro-elastic plates in contact with fluid, *Applied Mathematical Modelling* **37**: 2503-2515.
- [15] Alaimo A., Milazzo A., Orlando C., 2013, A four-node MITC finite element for magneto-electro-elastic multilayered plates, *Computers and Structures* **129**: 120-133.
- [16] Li Y.S., 2014, Buckling analysis of magneto-electro-elastic plate resting on Pasternak elastic foundation, *Mechanics Research Communications* **56**: 104-114.
- [17] Chang T.P., 2013, Deterministic and random vibration analysis of fluid-contacting transversely isotropic magneto-electro-elastic plates, *Computers and Fluids* **84**: 247-254.
- [18] Zhou Z.G., Wang B., Sun Y.G., 2004, Two collinear interface cracks in magneto-electro-elastic composites, *International Journal of Engineering Science* **42**: 1155-1167.
- [19] Li J.Y., 2000, Magneto-electro-elastic multi-inclusion and inhomogeneity problems and their applications in composite materials, *International Journal of Engineering Science* **38**: 1993-2011.
- [20] Milazzo A., 2014, Large deflection of magneto-electro-elastic laminated plates, *Applied Mathematical Modelling* **38**: 1737-1752.
- [21] Xue C.X., Pan E., 2013, On the longitudinal wave along a functionally graded magneto-electro-elastic rod, *International Journal of Engineering Science* **62**: 48-55.
- [22] Raeisifard H., Bahrami M.N., Yousefi-Koma A., Raeisi Fard H., 2014, Static characterization and pull-in voltage of a micro-switch under both electrostatic and piezoelectric excitations, *European Journal of Mechanics A/Solids* **44**: 116-124.
- [23] Mobki H., Sadeghi M.H., Rezazadeh G., Fathalilou M., Keyvani-janbaban A.A., 2014, Nonlinear behavior of a nano-scale beam considering length scale-parameter, *Applied Mathematical Modelling* **38**: 1881-1895.
- [24] Rezazadeh G., Madinei H., Shabani R., 2012, Study of parametric oscillation of an electrostatically actuated microbeam using variational iteration method, *Applied Mathematical Modelling* **36**: 430-443.
- [25] Zhang W.M., Yan H., Peng Z.K., Meng G., 2014, Electrostatic pull-in instability in MEMS/NEMS: A review, *Sensors and Actuators A: Physical* **214**: 187-218.
- [26] Khanchehgardan A., Rezazadeh G., Shabani R., 2014, Effect of mass diffusion on the damping ratio in micro-beam resonators, *International Journal of Solids and Structures* **51**: 3147-3155.
- [27] Khanchehgardan A., Shah-Mohammadi-Azar A., Rezazadeh G., Shabani R., 2013, Thermo-elastic damping in nano-beam resonators based on nonlocal theory, *International Journal of Engineering* **26**(12): 1505-1514.
- [28] Duan J.S., Rach R., 2013, A pull-in parameter analysis for the cantilever NEMS actuator model including surface energy, fringing field and Casimir effects, *International Journal of Solid and Structures* **50**: 3511-3518.
- [29] Taghavi N., Nahavi H., 2013, Pull-in instability of cantilever and fixed-fixed nano-switches, *European Journal of Mechanics A/Solids* **41**: 123-133.
- [30] Wang K.F., Wang B.L., 2014, Influence of surface energy on the non-linear pull-in instability of nano-switches, *International Journal of Non-linear Mechanics* **59**: 69-75.
- [31] Yu Y.P., Wu B.S., 2014, An approach to predicting static responses of electrostatically actuated micro-beam under the effect of fringing field and Casimir force, *International Journal of Mechanical Science* **80**: 183-192.

- [32] Zamanzadeh M., Rezazadeh G., Jafarsadeghi-poornaki I., Shabani R., 2013, Static and dynamic stability modeling of a capacitive FGM micro-beam in presence of temperature changes, *Applied Mathematical Modelling* **37**: 6964-6978.
- [33] Mobki H., Rezazadeh G., Sadeghi M., Vakili-Tahami F., Seyyed-Fakhrabadi M.S., 2013, A comprehensive study of stability in an electro-statically actuated micro-beam, *International Journal of Non-linear Mechanics* **48**: 78-85.
- [34] Osterberg P.M., Senturia S.D., 1997, M-test: A test chip for MEMS material property measurement using electrostatically actuated test structure, *Journal of Microelectromechanical Systems* **6** (2): 107-118.